Chinese Physics Letters **41**, 120302 (2024)

Locally purified density operators for noisy quantum circuits

Yuchen Guo[1] and Shuo Yang[1,2,3]*

[1]*State Key Laboratory of Low Dimensional Quantum Physics and Department of Physics, Tsinghua University, Beijing 100084, China*
[2]*Frontier Science Center for Quantum Information, Beijing 100084, China*
[3]*Hefei National Laboratory, Hefei 230088, China*

(Received 9 October 2024; accepted manuscript online 4 November 2024)

Open quantum system simulations are essential for exploring novel quantum phenomena and evaluating noisy quantum circuits. In this Letter, we investigate whether mixed states generated from noisy quantum circuits can be efficiently represented by locally purified density operators (LPDOs). We map an LPDO of N qubits to a pure state of size $2 \times N$ defined on a ladder and introduce a unified method for managing virtual and Kraus bonds. We numerically simulate noisy random quantum circuits with depths of up to $d = 40$ using fidelity and entanglement entropy as accuracy measures. The LPDO representation is effective in describing mixed states in both the quantum and classical regions; however, it encounters significant challenges at the quantum-classical critical point, restricting its applicability to the quantum region. In contrast, matrix product operators (MPO) successfully characterize the entanglement trend throughout the simulation, while the truncation in MPOs breaks the positivity condition required for a physical density matrix. This work advances our understanding of efficient mixed-state representations in open quantum systems and provides insights into the entanglement structure of noisy quantum circuits.

DOI: 10.1088/0256-307X/41/12/120302

Introduction. Simulating open quantum systems is crucial for theoretical and practical advancements,[1–7] because it enables the investigation of fascinating quantum phenomena in finite-temperature or dissipative systems[8–17] and plays a crucial role in evaluating the performance of noisy quantum circuits.[18–25] However, handling large open quantum systems is a formidable challenge because of the exponential growth of the density operator space. Efficiently representing mixed states is crucial for accurately simulating and analyzing noisy quantum circuits.

The traditional tensor network family,[26–30] which includes matrix product states (MPS)[31–33] and projected entangled pair states,[34–40] provides an intuitive understanding and compact representation of entanglement structures in many-body pure states with only a polynomial number of variational parameters and computational costs as the system size increases. In the realm of open quantum system simulation, the concept of locally purified density operators (LPDOs)[41–43] has found applications in the study of one-dimensional (1D) open systems governed by master equations,[44] noisy quantum circuit simulation,[23] quantum state or process tomography,[45–48] and topological quantum matter in open systems.[49] This raises the question of whether a mixed state can be efficiently represented by an LPDO, where the absence of an analytical conclusion hinders the reliability of related methods and algorithms.

In this Letter, we address this challenge by mapping an LPDO of N qubits to a pure state of size $2 \times N$ defined on a ladder, where the implementation of quantum gates and noise channels follows a similar framework. This unified approach facilitates the simultaneous management of both virtual and inner bonds, leading to the emergence of a critical scaling formula of circuit depth for an efficient LPDO representation, which constitutes the main theoretical contribution of this study. To verify this unified framework, we perform numerical simulations involving random noisy quantum circuits with a depth of up to $d = 40$. We evaluate the accuracy of capturing complex dynamics using the fidelity and entanglement entropy (EE) measures. Throughout the simulations, we observe two well-defined dynamic regions: a quantum region in which quantum entanglement continues to accumulate and a classical region in which the system gradually becomes fully depolarized, consistent with previous numerical results.[50–53] Both regions allow for an accurate LPDO approximation. However, the transition between these regions, the quantum-classical crossover point, poses a significant challenge to the classical simulation process, hindering the simulation of dynamics beyond the critical point.

LPDO Representation for Mixed States. We start from the MPS shown in Fig. 1(a) with two physical indices at each site

$$|\psi\rangle = \sum_{\{\boldsymbol{\tau},\boldsymbol{\kappa}\}} \sum_{\{\boldsymbol{\mu}\}} \prod_{j=1}^{N} [A_j]^{\tau_j,\kappa_j}_{\mu_{j-1},\mu_j} |\tau_1, \kappa_1, \cdots, \tau_N, \kappa_N\rangle, \quad (1)$$

where $\boldsymbol{\mu}$ denote virtual indices with dimension χ and $\boldsymbol{\kappa}$ denote Kraus indices with dimension d_κ. Tracing out all

*Corresponding author. Email: shuoyang@tsinghua.edu.cn
© 2024 Chinese Physical Society and IOP Publishing Ltd

Kraus indices yields the following mixed state:

$$\rho = \mathrm{Tr}_\kappa[|\psi\rangle\langle\psi|] = \sum_{\{\boldsymbol{\tau},\boldsymbol{\omega}\}} \sum_{\{\boldsymbol{\mu},\boldsymbol{\nu},\boldsymbol{\kappa}\}} \prod_{j=1}^{N} [A_j]^{\tau_j,\kappa_j}_{\mu_{j-1},\mu_j} [A_j^*]^{\omega_j,\kappa_j}_{\nu_{j-1},\nu_j} \cdot |\tau_1,\cdots,\tau_N\rangle\langle\omega_1,\cdots,\omega_N|, \quad (2)$$

as depicted in Fig. 1(b). Similar to the well-established connection between the locality of interaction and efficient MPS representation, local purification requires the locality between the system and environment, where system qubits only interact with adjacent ancillae.[54]

However, although virtual and Kraus indices are related to quantum entanglement and classical mixtures, respectively,[23] this interpretation is less straightforward than in MPS formalism. In the MPS context, virtual indices embody the Schmidt decomposition between different subsystems, and an entanglement area law ensures a constant bond dimension D.[31,55–57] In addition, from a purification perspective, d_κ equal to the physical bond dimension d_p is sufficient to represent any mixed state exactly but requires a large χ that may grow exponentially with the system size. However, selecting a larger d_κ can reduce χ and overall complexity while maintaining accuracy. This implies that these two inner indices should be considered together, as illustrated in the following discussion.

A general mixed state allows for an eigenvalue decomposition as $\rho = \sum_k \lambda_k |\psi_k\rangle\langle\psi_k|$, which naturally corresponds to an unnormalized supervector in double space $|\rho\rangle\rangle = \sum_k \lambda_k |\psi_k\rangle \otimes |\psi_k^*\rangle$. In this way, a 1D mixed state with N qubits can be converted into a quasi-1D system of size $2 \times N$. In particular, the density operator ρ represented by the LPDO can be regarded as a $2 \times N$ state on a ladder, as shown in Fig. 1(c). Therefore, an efficient LPDO representation of the original mixed state requires the corresponding supervector to satisfy the entanglement area law.

Entanglement Dynamics in Noisy Quantum Circuits. Here, we investigate the entanglement dynamics of Kraus and virtual indices in a general noisy quantum circuit. As shown in Fig. 1(c), a division line of length L splits the entire state into two regions, requiring $O(L)$ scaling of the EE between the two subsystems to ensure an efficient tensor network representation. Therefore, it is important to investigate the contributions of these basic components of a noisy quantum circuit, namely, unitary gates and noise channels, to this bipartite entanglement measure. Note that to obtain a reasonable estimate of the von Neumann EE, the supervector should be renormalized as $\langle\langle\rho|\rho\rangle\rangle = \mathrm{Tr}[\rho^2] = 1$.

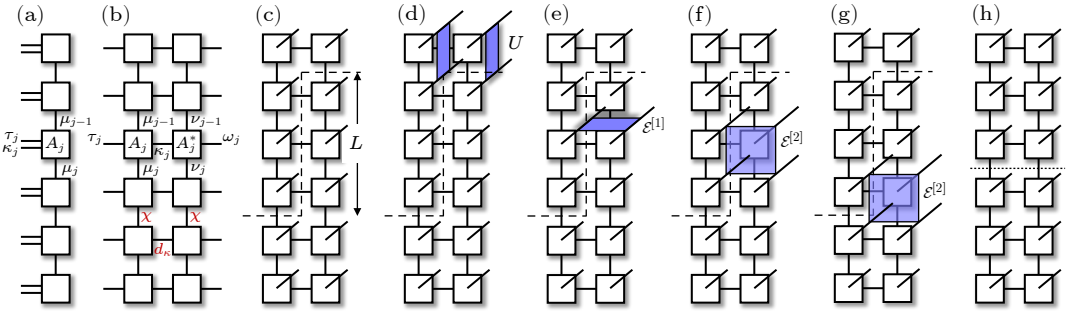

Fig. 1. (a) Purified state of LPDO. (b) Mixed state in its LPDO representation. (c) Corresponding supervector on ladder. (d-g) Implementation of quantum circuit in mixed state. (d) Implementation of two-qubit gate. (e) Implementation of single-qubit noise. (f, g) Implementation of two-qubit noise. (h) Division of half-cut EE used in numerical simulations.

Detailed analysis of the roles of different gates and noise channels is provided in Supplemental Material,[54] where the results are summarized as follows:

- **Single-qubit unitary gates.** These gates do not alter the entanglement structure, i.e., $\Delta S = 0$.
- **Two-qubit unitary gates.** One possible position for a two-qubit unitary gate to cross the division line is illustrated in Fig. 1(d), suggesting that a layer of two-qubit gates increases entanglement by at most $\Delta S \leq 2C_U$.
- **Single-qubit noise.** A single-qubit noise channel [Fig. 1(e)] exhibits little difference from the two-qubit unitary gate in this framework. Consequently, a layer of single-qubit noise channels induces a change in entanglement that satisfies $\Delta S \leq LC_{\mathcal{E}}^{[1]}$.
- **Two-qubit noise.** Similarly, a layer of two-qubit noise channels intersects the division by $L+1$ times, as shown in Fig. 1(f) and 1(g), increasing the entanglement of $\Delta S \leq (L+1)C_{\mathcal{E}}^{[2]}$.

Here, C_U denotes a constant of order $O(1)$ that describes the capacity of a unitary gate to generate entanglement in a normal quantum state. In addition, $C_{\mathcal{E}}^{[i]}$ is proportional to the error rate $\varepsilon^{[i]}$ of the corresponding i-qubit gates.

In summary, for a quantum circuit with a staggered arrangement of single- and two-qubit gates (where the two-qubit gates form a brick-wall structure),[45,54] the entanglement growth under the circuit depth d can be estimated as follows:

$$\Delta S \leq \frac{d}{2}(2C_U + LC_{\mathcal{E}}^{[1]} + (L+1)C_{\mathcal{E}}^{[2]}) \sim O(d\varepsilon L), \quad (3)$$

which is satisfied for large L. Consequently, the supervector $|\rho\rangle\rangle$ for a mixed state generated from a noisy circuit

with a depth scaling lower than $d \sim \varepsilon^{-1}$ satisfies $S \lesssim O(L)$. This depth scaling ensures an efficient tensor network representation for $|\rho\rangle\rangle$; thus, an efficient LPDO representation for ρ is obtained. In other words, we expect failure in the LPDO simulation when the circuit is deeper than the scaling behavior $d \sim \varepsilon^{-1}$, which is irrelevant to the concrete unitary gates used in the circuit. In addition, this theoretical prediction applies to a general gate configuration when considering the relative density of gates p compared to the brick-wall case to define an effective error rate $p\varepsilon$, as demonstrated in the following numerical experiments.

Numerical Simulations for Noisy Quantum Circuits. In our numerical simulations, we use brick-wall circuits with Haar-random two-qubit gates[54,58,59] accompanied by two-qubit depolarizing noise. Initially, we focus on systems with $N = 8$ qubits whose entire dynamics can be simulated exactly as a benchmark. We evaluate supervector fidelity, defined as $f(|\rho_1\rangle\rangle, |\rho_2\rangle\rangle) \equiv \langle\langle\rho_1|\rho_2\rangle\rangle$ with $\langle\langle\rho_i|\rho_i\rangle\rangle = 1$,[54] between the matrix product operator (MPO) or LPDO and exact diagonalization (ED) in Fig. 2(a) for different two-qubit error rates ε. The MPO truncation follows the conventional method,[50] whereas we improve the LPDO truncation method to improve accuracy and robustness.[54]

First, for a typical $\varepsilon = 0.01$ of state-of-the-art quantum hardware, we observe a region where LPDO with $\chi = 16$ and $d_\kappa = 2$ (red circles) exhibits expressive power comparable to that of an MPO with $D = \chi^2 = 256$ (gray crosses, exact for $N = 8$) and better than $D = \chi^2/2 = 128$ (gray triangles) up to depth $d = 33$, whereas the LPDO structure consumes significantly fewer computational resources ($d_p^2 D^2$) than the MPO structure ($d_p d_\kappa \chi^2$). This region is smaller for stronger noise when comparing the upper and lower panels of Fig. 2(a). Therefore, our results highlight the importance of selecting an appropriate ansatz when simulating noisy circuits at different error rates ε.

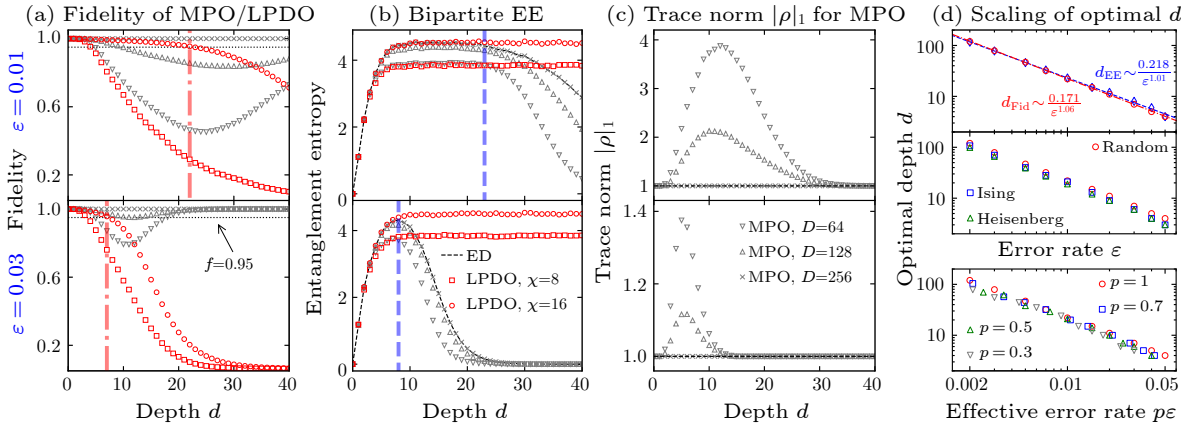

Fig. 2. (a-c) Dynamics of noisy quantum circuits with $N = 8$ for ED, MPO with different D values, and LPDO with $d_\kappa = 2$ and different χ values, sharing the same legend. The upper and lower panels show the results for $\varepsilon = 0.01$ and $\varepsilon = 0.03$, respectively. (a) Fidelity between the ED and MPO/LPDO results. The red dashed lines indicate the positions where $f_{\rm LPDO}$ ($\chi = 16$, $d_\kappa = 2$) decreases below 0.95. (b) Bipartite EE values for different methods. The blue dashed lines indicate the positions where $\mathrm{EE}_{\rm ED}$ and $\mathrm{EE}_{\rm LPDO}$ ($\chi = 16$, $d_\kappa = 2$) deviate by more than 3%. (c) Trace norm $|\rho|_1$ for MPO with different D values. (d) The 'optimal depth' for the LPDO simulation under different ε values. The upper panel: $d_{\rm opt}$ determined by the fidelity and EE for random gates. The middle panel: $d_{\rm opt}$ determined by the fidelity for different gates, including random gates and the time evolution of two spin models. The lower panel: $d_{\rm opt}$ determined by the fidelity for random gates, where each gate is randomly preserved with probability p.

Nevertheless, it is crucial to note that with the accumulation of noise, an LPDO can no longer accurately capture the exact trajectories due to significant decoherence effects after a characteristic depth. This 'optimal depth', defined as the point where the fidelity between ED and LPDO with $\chi = 16$ and $d_\kappa = 2$ drops below $f = 0.95$, is represented by red dashed lines in Fig. 2(a) and fitted as $d_{\rm Fid} \sim 0.171/\varepsilon^{1.06}$ in the upper panel of Fig. 2(d). These results reveal the failure of the LPDO simulation beyond this optimal depth, thereby validating our theoretical analysis and prediction based on Eq. (3). In addition, this result is independent of the concrete two-qubit unitary gates and their configuration, as demonstrated by the collapse across different gates, including random gates and time evolution of two spin models, as well as different configurations achieved by randomly preserving each gate with probability p (resulting in an effective error rate of $p\varepsilon$[54]), as shown in the middle and lower panels of Fig. 2(d), respectively. This result suggests the universality of our theoretical formalism in Eq. (3), indicating that the optimal depth is determined solely by the effective noise strength, regardless of the unitary gates involved.

To understand the physical interpretation of the optimal depth, we compare the bipartite EE of the supervector $|\rho\rangle\rangle$ [divided into half of the chain, as shown in Fig. 1(h)] for the simulations of ED, MPO, and LPDO in Fig. 2(b). We observe an increasing-decreasing trend in EE from the ED simulation, dividing the entire dynamics into two regions: (1) a quantum region in which quantum entanglement gradually accumulates, potentially offering quantum advantages for systems with significantly larger sizes; (2) a classical region dominated by noise effects, leading to highly depolarized and mixed systems, consistent with the numerical results of recent works.[50–52] Even after trunca-

tion, the MPO simulation qualitatively captures this trend, whereas the LPDO simulation only accurately describes the EE dynamics in the quantum region. In other words, the failure of the LPDO simulation occurs at the critical point when the circuit EE starts to decrease from its maximal value and transitions into the classical region. We mark this critical point, defined as the point where the EE of an LPDO with $\chi = 16$ and $d_\kappa = 2$ and ED differ by more than 3%, by blue dashed lines in Fig. 2(b) and fitted in the upper panel of Fig. 2(d), consistent with the optimal point defined by the previously described fidelity. This implies that the intricate interplay between entanglement and noise in the quantum-classical crossover region leads to the failure of the LPDO simulation.

However, although the MPO simulation effectively captures the overall trend of the EE dynamics in both regimes, it may violate the positivity condition for a physical density matrix that cannot be imposed on the local tensor of an MPO. To comprehensively assess the MPO performance, we calculate the trace norm $|\rho|_1$ for a normalized MPO with $\mathrm{Tr}(\rho) = 1$. This measure, which is the summation of all singular values, exceeds 1 if the density operator has negative components. The results presented in Fig. 2(c) reveal that after truncation, which is inevitable for simulating larger systems with finite depths D, the MPO fails to preserve the positivity condition. In addition, we observe that the maximal 'negativity' occurs before the critical point, suggesting a potential causal relationship between these two issues and offering additional insights into the difficulty of the LPDO at the critical point.

In our previous analysis, we primarily focused on the entanglement structure when deriving the critical scaling, which serves as a necessary condition for the LPDO representation. However, due to its inherent structure that aims to preserve local positivity, the efficacy of the LPDO representation even with infinite d_κ may be limited compared to the MPO representation that lacks such constraints. Therefore, we anticipate that the failure of the LPDO structure follows the peaks of MPO negativity, where there is a crucial trade-off between the accuracy of the observables and the positivity of the output states. This conflict cannot be alleviated only by increasing d_κ, as illustrated in Fig. S4.[54] Fortunately, with the development of quantum hardware, only dynamics in the quantum region can demonstrate a quantum advantage, where LPDOs can capture long-time dynamics of interest and significantly outperform MPOs in terms of both accuracy and efficiency, as demonstrated in the 'weak-noise' case (Fig. S6[54]).

Projection to LPDO. To further explore the properties of these dynamic critical points and explain the limitations of the LPDO simulation in this context, we propose a gradient descent algorithm to project an MPO onto an LPDO. Specifically, we optimize the following loss function:

$$\Theta = ||\rho - \rho'||_F^2 = \mathrm{Tr}[\rho^2 + \rho'^2 - 2\rho\rho'], \tag{4}$$

where ρ denotes the original MPO and ρ' denotes the approximated LPDO. To obtain an approximated LPDO ρ' with a minimal loss Θ, we performed gradient descent using the Adam optimizer.[60]

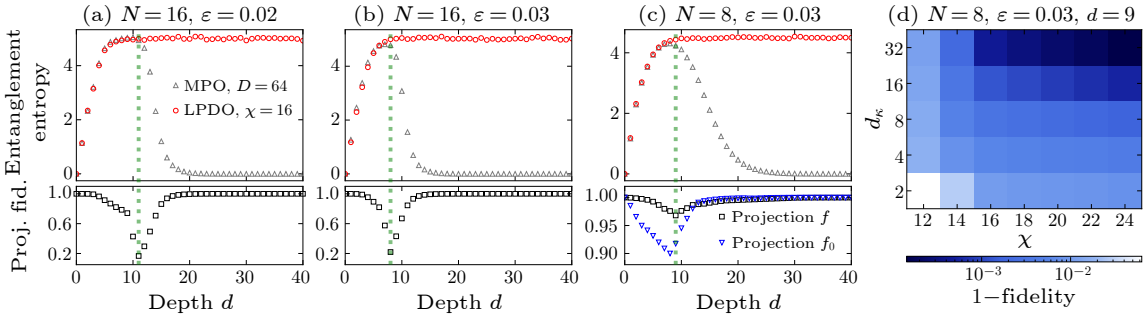

Fig. 3. Projection fidelity for projection from MPO to LPDO compared with EE dynamics simulated by both structures. (a-c) The upper panels show the EE values for noisy circuits with different N and ε values. The lower panels show the fidelity of projecting MPO with $D = 256$ onto LPDO with $\chi = 16$ and $d_\kappa = 2$. The green dotted line indicates the minimum fidelity position. The conventional fidelity f_0 for mixed states and the supervector fidelity f are compared in (c). (d) Projection from MPO with $D = 256$ generated from noisy circuits with $N = 8$, depth $= 9$, and $\varepsilon = 0.03$ to LPDO with different χ and d_κ values.

Figures 3(a)–3(c) plot the projection fidelity from the simulated MPO at each depth with $D = 256$ to an LPDO with fixed $\chi = 16$ and $d_\kappa = 2$ for different N and ε [distinct from the fidelity for LPDO simulation shown in Fig. 2(a)], along with the directly simulated LPDO EE with the same d_κ and χ for visualization of the critical point discussed previously. Here, we consider both the density matrix fidelity f_0 and the supervector fidelity f [Fig. 3(c)] for $N = 8$,[54] where the results reveal a similar trend for these two fidelity measures. The minimum fidelity is observed around the critical point where the EE estimated by the MPO and LPDO deviate, indicating a fundamental limitation of the LPDO representation in that region. Furthermore, the deviation from the correct trajectory for the dynamics near the critical point hinders the LPDO simulation at and after that point because the LPDO trajectory cannot be directly corrected back to its original dynamics once destroyed. Therefore, although the mixed states in the classical region can be well approximated by LPDOs, LPDO simulations cannot reach those states, leading to the difference between Fig. 2(a) and Fig. 3.

The overall trends of the projection fidelity in Fig. 3(b) and 3(c) are similar; however, the values around the critical point for $N = 16$ are significantly less than $N = 8$,

where an exact MPO representation is available. This unsatisfactory fidelity can attributed to the MPO truncation during the simulation that introduces nonpositive parts, as shown in Fig. 2(c). This indicates a difference between the LPDO with χ and the MPO with $D = \chi^2$ in their representative capacities for highly compressed mixed states, where adherence to the positivity condition is most challenging. This highlights the difficulty of LPDOs in accurately capturing dynamics under stringent positivity constraints.

Finally, we compare the expressive capacities of LPDOs with different χ and d_κ values for noisy quantum states. To avoid the truncation of the MPO representation that may lead to the aforementioned nonphysical properties, we adopt $N = 8$ and directly implement the projection from the exact density matrices generated from the noisy circuits with $\varepsilon = 0.03$ and $d = 9$ to an LPDO at the critical point between the quantum and classical regions. From the projection fidelity shown in Fig. 3(d), we observe that, for example, an LPDO with $\chi = 24$ and only $d_\kappa = 4$ can possess a representative power similar to that of an LPDO with $\chi = 14$ but significantly larger d_κ, at least for the quantum states generated from the typical noisy quantum circuits of interest. This implies that the difference between virtual and Kraus indices is not absolute, and a unified scheme to treat them according to our proposal is reasonable.

Conclusion and Discussion. In conclusion, our investigation into the simulation of open quantum systems via the LPDO representation has clarified its capacity and limitations when dealing with the dynamics of noisy quantum circuits. Through theoretical predictions and numerical simulations, we observe a critical point between the quantum and classical regions, which remains a challenge for LPDO representation, as evidenced by the divergence in EE from the exact results and the minimal fidelity of the projection.

This study offers several implications. First, the universality of the critical scaling embodied in Eq. (3), highlighted by the consistency across various unitary gates and circuit configurations, provides a strategic approach for estimating the optimal depth of any quantum circuit. Specifically, the corresponding scaling coefficient can be determined based on an arbitrary error rate ε, by, e.g., conducting an MPO simulation once; then, the quantum region conducive to the LPDO simulation can be identified. Consequently, continued MPO simulation becomes unnecessary, because LPDO suffices to characterize the dynamics in the quantum region, whereas the classical regime diminishes in relevance with little quantum advantage. Our results delineate the application scope of these LPDO-based quantum state and process tomography methods[46–48] based on the predicted optimal depth.

Further exploration and characterization of the interplay between noise effects and quantum entanglement, particularly in the crossover between the quantum and classical regions, are essential.[61] Possible connections to these measurements, noise-induced phase transitions,[62–67] or other dynamic phase transitions[68–72] are also interesting. In summary, the challenges and opportunities identified in this study provide a foundation for further research into the efficient representation and simulation of open quantum states, providing potential advances in quantum information processing and quantum computing.

Acknowledgements. This work was supported by the National Natural Science Foundation of China (Grant Nos. 12174214, 12475022, and 92065205) and the Innovation Program for Quantum Science and Technology (Grant No. 2021ZD0302100).

References

[1] Breuer H P and Petruccione F 2007 *The Theory of Open Quantum Systems* (Oxford University Press)
[2] Rivas Á and Huelga S F 2012 *Open Quantum Systems: An Introduction*, 1st ed. (Springer Berlin, Heidelberg)
[3] Hofer P P, Perarnau-Llobet M, Miranda L D M, Haack G, Silva R, Brask J B, and Brunner N 2017 *New J. Phys.* **19** 123037
[4] Cattaneo M, De Chiara G, Maniscalco S, Zambrini R, and Giorgi G L 2021 *Phys. Rev. Lett.* **126** 130403
[5] Schlimgen A W, Head-Marsden K, Sager L M, Narang P, and Mazziotti D A 2021 *Phys. Rev. Lett.* **127** 270503
[6] Liu H Y, Sun T P, Wu Y C, and Guo G P 2021 *Chin. Phys. Lett.* **38** 080301
[7] Kamakari H, Sun S N, Motta M, and Minnich A J 2022 *PRX Quantum* **3** 010320
[8] Weiss U 2012 *Quantum Dissipative Systems*, 4th ed. (World Scientific)
[9] Kessler E M, Giedke G, Imamoglu A, Yelin S F, Lukin M D, and Cirac J I 2012 *Phys. Rev. A* **86** 012116
[10] Walter S, Nunnenkamp A, and Bruder C 2014 *Phys. Rev. Lett.* **112** 094102
[11] Xu M, Tieri D A, Fine E C, Thompson J K, and Holland M J 2014 *Phys. Rev. Lett.* **113** 154101
[12] Kimchi-Schwartz M E, Martin L, Flurin E, Aron C, Kulkarni M, Tureci H E, and Siddiqi I 2016 *Phys. Rev. Lett.* **116** 240503
[13] Keßler H, Kongkhambut P, Georges C, Mathey L, Cosme J G, and Hemmerich A 2021 *Phys. Rev. Lett.* **127** 043602
[14] de Groot C, Turzillo A, and Schuch N 2022 *Quantum* **6** 856
[15] Ma R and Wang C 2023 *Phys. Rev. X* **13** 031016
[16] Ma R, Zhang J H, Bi Z, Cheng M, and Wang C 2023 arXiv:2305.16399 [cond-mat.str-el]
[17] Zhang J H, Ding K, Yang S, and Bi Z 2023 *Phys. Rev. B* **108** 155123
[18] Nielsen M A and Chuang I L 2010 *Computation and Quantum Information* (Cambridge University Press)
[19] Bremner M J, Montanaro A, and Shepherd D J 2017 *Quantum* **1** 8
[20] Preskill J 2018 *Quantum* **2** 79
[21] Sarovar M, Proctor T, Rudinger K, Young K, Nielsen E, and Blume-Kohout R 2020 *Quantum* **4** 321
[22] von Lüpke U, Beaudoin F, Norris L M, Sung Y, Winik R, Qiu J Y, Kjaergaard M, Kim D, Yoder J, Gustavsson S, Viola L, and Oliver W D 2020 *PRX Quantum* **1** 010305
[23] Cheng S, Cao C, Zhang C, Liu Y, Hou S Y, Xu P, and Zeng B 2021 *Phys. Rev. Res.* **3** 023005
[24] Cattaneo M, Rossi M A C, García Pérez G, Zambrini R, and Maniscalco S 2023 *PRX Quantum* **4** 010324
[25] Torre E G D and Roses M M 2023 arXiv:2308.01339 [quant-ph]
[26] Verstraete F, Murg V, and Cirac J I 2008 *Adv. Phys.* **57** 143
[27] Orús R 2014 *Ann. Phys.* **349** 117
[28] Bridgeman J C and Chubb C T 2017 *J. Phys. A* **50** 223001
[29] Cirac J I, Pérez-García D, Schuch N, and Verstraete F 2021 *Rev. Mod. Phys.* **93** 045003
[30] Bai S C, Tang Y C, and Ran S J 2022 *Chin. Phys. Lett.* **39** 100701

[31] Verstraete F and Cirac J I 2006 *Phys. Rev. B* **73** 094423
[32] Pérez-García D, Verstraete F, Wolf M M, and Cirac J I 2007 *Quantum Inf. Comput.* **7** 401
[33] Schollwöck U 2011 *Ann. Phys.* **326** 96
[34] Verstraete F, Wolf M M, Perez-Garcia D, and Cirac J I 2006 *Phys. Rev. Lett.* **96** 220601
[35] Schuch N, Wolf M M, Verstraete F, and Cirac J I 2007 *Phys. Rev. Lett.* **98** 140506
[36] Schuch N, Cirac I, and Pérez-García D 2010 *Ann. Phys.* **325** 2153
[37] Cirac J I, Poilblanc D, Schuch N, and Verstraete F 2011 *Phys. Rev. B* **83** 245134
[38] Schuch N, Poilblanc D, Cirac J I, and Pérez-García D 2013 *Phys. Rev. Lett.* **111** 090501
[39] Yang S, Lehman L, Poilblanc D, Van Acoleyen K, Verstraete F, Cirac J I, and Schuch N 2014 *Phys. Rev. Lett.* **112** 036402
[40] Yang S, Wahl T B, Tu H H, Schuch N, and Cirac J I 2015 *Phys. Rev. Lett.* **114** 106803
[41] Verstraete F, García-Ripoll J J, and Cirac J I 2004 *Phys. Rev. Lett.* **93** 207204
[42] Zwolak M and Vidal G 2004 *Phys. Rev. Lett.* **93** 207205
[43] las Cuevas G D, Schuch N, Pérez-García D, and Cirac J I 2013 *New J. Phys.* **15** 123021
[44] Werner A H, Jaschke D, Silvi P, Kliesch M, Calarco T, Eisert J, and Montangero S 2016 *Phys. Rev. Lett.* **116** 237201
[45] Guo Y and Yang S 2022 *PRX Quantum* **3** 040313
[46] Guo Y and Yang S 2024 *Commun. Phys.* **7** 322
[47] Li W J, Xu K, Fan H, Ran S J, and Su G 2023 arXiv:2308.06900 [quant-ph]
[48] Torlai G, Wood C J, Acharya A, Carleo G, Carrasquilla J, and Aolita L 2023 *Nat. Commun.* **14** 2858
[49] Guo Y, Zhang J H, Yang S, and Bi Z 2024 arXiv:2403.16978 [cond-mat.str-el]
[50] Noh K, Jiang L, and Fefferman B 2020 *Quantum* **4** 318
[51] Li Z, Sang S, and Hsieh T H 2023 *Phys. Rev. B* **107** 014307
[52] Zhang M, Wang C, Dong S, Zhang H, Han Y, and He L 2022 *Phys. Rev. A* **106** 052430
[53] Zhang Q and Zhang G M 2022 *Chin. Phys. Lett.* **39** 050302
[54] See supplemental material for details.
[55] Bravyi S, Hastings M B, and Verstraete F 2006 *Phys. Rev. Lett.* **97** 050401
[56] Hastings M B 2007 *J. Stat. Mech.: Theory Exp.* **2007** P08024
[57] Eisert J, Cramer M, and Plenio M B 2010 *Rev. Mod. Phys.* **82** 277
[58] Nahum A, Ruhman J, Vijay S, and Haah J 2017 *Phys. Rev. X* **7** 031016
[59] Fisher M P A, Khemani V, Nahum A, and Vijay S 2023 *Annu. Rev. Condens. Matter Phys.* **14** 335
[60] Kingma D P and Ba J 2017 arXiv:1412.6980 [cs.LG]
[61] Guo Y and Yang S 2023 *npj Quantum Inf.* **9** 11
[62] Li Y, Chen X, and Fisher M P A 2018 *Phys. Rev. B* **98** 205136
[63] Skinner B, Ruhman J, and Nahum A 2019 *Phys. Rev. X* **9** 031009
[64] Li Y, Chen X, and Fisher M P A 2019 *Phys. Rev. B* **100** 134306
[65] Vasseur R, Potter A C, You Y Z, and Ludwig A W W 2019 *Phys. Rev. B* **100** 134203
[66] Yang Z C, Li Y, Fisher M P A, and Chen X 2022 *Phys. Rev. B* **105** 104306
[67] Guo Y, Zhang J H, Bi Z, and Yang S 2023 *Phys. Rev. Res.* **5** 043069
[68] Diehl S, Tomadin A, Micheli A, Fazio R, and Zoller P 2010 *Phys. Rev. Lett.* **105** 015702
[69] Zhang J, Pagano G, Hess P W, Kyprianidis A, Becker P, Kaplan H, Gorshkov A V, Gong Z X, and Monroe C 2017 *Nature* **551** 601
[70] Heyl M 2018 *Rep. Prog. Phys.* **81** 054001
[71] Muniz J A, Barberena D, Lewis-Swan R J, Young D J, Cline J R K, Rey A M, and Thompson J K 2020 *Nature* **580** 602
[72] Marino J, Eckstein M, Foster M S, and Rey A M 2022 *Rep. Prog. Phys.* **85** 116001